Journal of Engineering Mathematics **39:** 25–46, 2001.

Current-voltage characteristics from an asymptotic analysis of the MOSFET equations

ELLIS CUMBERBATCH, HENOK ABEBE and HEDLEY MORRIS[1]
Claremont Graduate University, Claremont, CA 91711, U.S.A.
[1]*San Jose State University, San Jose, CA 95192, U.S.A.*

Received 17 September 1999; accepted in revised form 21 August 2000

Abstract. Phenomenological formulae for the current-voltage characteristics of a MOSFET are derived by extending the asymptotic method of Ward. Practical methods for combining the perturbation approximations and numerically implementing the Ward equations are developed. A detailed comparison with real MOSFET data is presented and the model is shown to be effective over a range of device geometries.

Key words: semiconductor modeling, asymptotic analysis, MOSFET current/voltage formulae, comparison with data.

1. Introduction

A semiconductor chip is made by fabricating up to 10^6 transistors and their inter-connections on the surface of a silicon wafer. The transistors are usually MOSFET's (metal-oxide-silicon-field-effect-transistors), drawn from a small set of designs (n-type, p-type) and of various sizes (lengths and widths). Each chip has circuit functions, and in order to design the circuits using the transistor building blocks, the VLSI industry uses a program called SPICE. SPICE is the most common program for the simulation of electronic circuits. The original SPICE was developed in 1971 at U.C. Berkeley, and updated versions exist in many forms both commercial and public domain. See [1] for more information. For SPICE to produce a design, the software must access the current/voltage relation for *each* transistor a number of times. In order that this be effected in a reasonable time, the current/voltage relationships for the transistors must have simple form.

The classical approximation governing the flow of electrons and holes in a semi-conductor relevant to the low field-strength operation of a transistor has been in use for over forty years [2, 3]. It results in a set of nonlinear partial differential equations for the electron density, n, the hole density, p, and the electric field, $\mathbf{E}$. Even in the time-independent case, which will be considered here and which is sufficient for many applications, the nonlinear character and the non-trivial geometry of the MOSFET preclude approaches that would generate exact solutions, least of all any that lead to simple current/voltage relationships. Hence there has resulted a variety of approximate solutions. A typical MOSFET geometry is shown in Figure 1.

The first approximation, which allows a reduction from a PDE system to an ODE system has the designation 'long channel' or 'quasi-one-dimensional' (called 1-D in the sequel). As indicated, this approximation has validity when the channel length, L, is relatively large. (See Figure 1 for the coordinate system, for identification of various regions on the device, etc. Also refer to Appendices A, B for variable definitions.) When voltages are applied at the gate

and/or drain, electrons and holes are attracted or repelled from these locations. The depletion region, bereft of either electrons or holes, plays an important role; a measure of its size is $L_D(\log\lambda/\lambda)^{\frac{1}{2}}$ where L_D is the Debye length and λ is a measure of the doping level relative to the intrinsic level. (λ is large, typically 10^6–10^7.) The ratio of these lengths, which plays the role of the aspect ratio of the device, is

$$\epsilon = \frac{L_D}{L}\sqrt{\frac{\log\lambda}{\lambda}}. \tag{1}$$

When ϵ is small most of the region under the gate is uniform in the x_2 -direction and the 1-D approximation is exact for the fields there; the approximation breaks down in the source-gate and drain-gate corners where the fields lose their 1-D character. When ϵ is large the corner regions influence the solution across the whole gate region and a two-dimensional solution is required. Ward [4], made the 1-D approximation into an explicit asymptotic expansion by scaling x_2, the variable along the channel, with L, and scaling x_1, the perpendicular variable, with L_D. Series expansions in powers of ϵ^2 give the 1-D approximation as the leading term of these series. In a subsequent paper [5], Ward obtained some solutions for the corner regions and matched them to the 1-D approximation in the central region under the gate. This enhanced solution would be expected to be more accurate down to smaller channel lengths, but the solution obtained is restricted to small drain voltages. For a typical device $L_D = 33$ microns, $\lambda = 10^6$, and for $L = 10$ microns, $\epsilon = 0{\cdot}012$. For ϵ this small we expect the 1-D approximation to be accurate; this is borne out by the data. However we show that by adjustments of some of the parameters we can make the 1-D approximation match the data at much reduced channel lengths. At the time of writing, the standard industry channel length is 0·25 micron, and the SPICE software, based on the 1-D approximation (but improved empirically), is still being used.

The 1-D approximation has the descriptor ‘quasi’ because the ODE in the x_1 direction contains x_2 as a parameter via the quasi-Fermi potential, φ. The electric potential, ψ, satisfies the second-order nonlinear ODE in x_1, which contains φ, and therefore its solution depends on x_2 parametrically. The form of $\varphi(x_2)$ is determined subsequently when the current flowing across the device is calculated. The ODE allows one integration in the case of constant doping. The current can then be expressed as a double integral called the Pao-Sah integral, see [6]. An approximation allows reduction to a single integral [7]. Further approximations valid over different regimes of the applied voltages V_{ds}, V_{gs} then yield explicit formulae for $I_{ds}(V_{ds}, V_{gs})$. These latter approximations are motivated by neglect of various physical effects in one or other regimes of operation. A comprehensive survey of these approximations and their inter-relations is found in [3] and [8]. These separate formulae, valid over distinct ranges of voltages, were found to be accurate for long channel use. As the need for denser packing of transistors on chips has intensified, and the technology has been able to satisfy those needs by reducing lengths and widths of transistors, these formulae have been adapted in various ways for use at the reduced sizes. Often these adaptations are little more than ‘fudge factors’, which have parameters valid only over limited ranges of size and voltage regimes. Hence these parameters are changed regime to regime (‘binning’). Current technology uses of the order of 150–200 parameters for $I_{ds}(V_{ds}, V_{gs})$ formulae for use in SPICE. Most of these parameters are not universal constants, and they must be ‘identified’ for each fabrication batch. This means considerable testing and data collection, followed by numerical optimization for parameter identification. All of this is expensive, both in time and money. There are pressures to improve the models so that they are less cumbersome and based more on physics. The

work reported here, done by the Claremont Graduate University Mathematics Clinic for the Information Sciences Institute MOSIS Program, has these more efficient models as its goal. Related goals were (a) comparison of the asymptotic results with data to determine the domain of validity of the asymptotic approximations, and (b) improvement of solution 'blending' by which solutions valid over different voltage regimes are patched together.

The work presented in here generates explicit $I_{ds}(V_{ds}, V_{gs})$ formulae based on the 1-D approximation. It takes further the asymptotic results for large λ derived by Ward in [4, 5]. These results in turn were based on the asymptotic scheme originated by Please, [9], for the $p - n$ junction. This scheme, based on the matched asymptotic expansion concept [10], obtains solutions valid in different regions and matches them across overlapping regions to provide a composite expansion valid over the whole region (to the order computed). In the 1-D MOSFET approximation there are three main regions: the inversion layer, a thin boundary layer containing a profusion of holes or electrons under some voltage regimes, the depletion layer, and the substrate which is determined by conditions far from the channel. The separate solutions in these regions are, by themselves, not difficult to obtain. However, matching them, and satisfying the boundary condition at the gate, are non-trivial exercises. Ward successfully accomplished these, in [4] for constant doping and for variable doping of constant signature, and in [5] for variable doping of opposite signature. Reference [11] presents the Ward analysis, and refers to other problems treated both asymptotically and numerically among a broad introduction to an advanced treatment of the semi-conductor equations.

The asymptotic solution achieved by Ward requires numerical work (to solve non-linear transcendental equations) and the $I_{ds}(V_{ds}, V_{gs})$ formula remains an integral to be computed numerically. Hence its use in the semi-conductor industry (via SPICE) is precluded. We briefly outline Ward's asymptotic results, and in Section 3 we show how the Ward analysis may be taken further (in the constant doping case) to achieve an *explicit* $I_{ds}(V_{ds}, V_{gs})$ formula. Part of our analysis is justifiable as a continuation of the asymptotics and it agrees with the numerical solution of the exact ODE/BC system. A second approximation is not justifiable asymptotically. It approximates by a constant a function that is varying inside an integral; with this, though, the integral can be evaluated analytically, and the two approximations combined to produce a formula for the current.

2. Equations, boundary conditions, and the quasi-1-D asymptotic approximation

Voltages may be applied at the source, drain, gate and substrate contacts (S, D, G, B in Figure 1); we shall assume that the substrate and source are at the same voltage. The voltages drain-to-source and gate-to-source are denoted by V_{ds}, V_{gs}, respectively. We shall treat an n-channel device (in inversion the channel is profuse in electrons). Here the silicon has been doped with acceptor atoms (typically the number ionized is $N_A^- \sim 10^{16} - 10^{17}$). Source, drain regions have been overlaid with donor atoms ($N_D^+ \sim 10^{19}$). An insulated layer (silicon dioxide) separates the gate contact from the silicon. As the gate voltage is raised, holes are repelled from the region under the gate, creating a depleted region. Further increase in V_{gs} attracts electrons to the insulator-substrate interface, creating the 'channel'. Voltages at the drain then cause a current to flow from source to drain. The aim of analysis of the device is to obtain the current created by this flow of electrons, I_{ds}, as a function of the applied voltages V_{ds} and V_{gs}. In addition, I_{ds} also depends on the parameters of the device: its size, the doping levels, the mobility of electrons, etc.

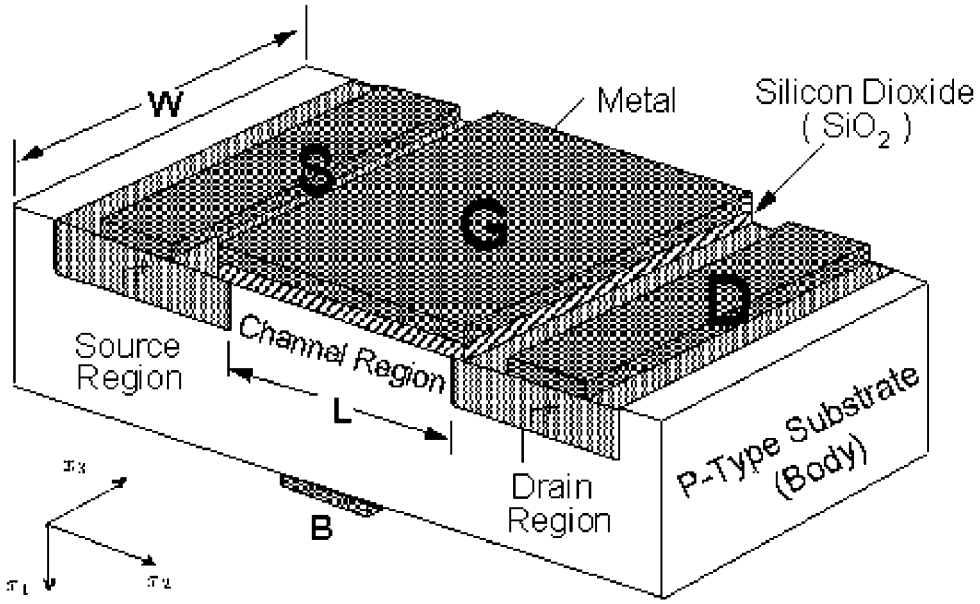

Figure 1. A schematic diagram of a MOSFET.

The standard model for the MOSFET comprises Gauss' equation for charge

$$\epsilon_s \nabla \cdot \mathbf{E} = -\rho = q(p - n + N), \tag{2}$$

together with the drift-diffusion model for the motion of electrons

$$\mathbf{J}_n = q\mu_n \left(\frac{kT}{q} \nabla n + n\mathbf{E} \right) \tag{3}$$

and the static conservation equation with no recombination/generation for the flux of electrons

$$\nabla \cdot \mathbf{J}_n = 0. \tag{4}$$

The assumption that the holes remain in thermal equilibrium allows the hole density to be obtained as

$$p = n_i \mathrm{e}^{-q\frac{\psi}{kT}}. \tag{5}$$

It is convenient to write

$$n = n_i \mathrm{e}^{q\frac{\psi - \varphi_n}{kT}} \tag{6}$$

with φ_n replacing n as a primary variable; it is called the quasi-Fermi potential. For other notation and definitions see Appendix A.

The boundary conditions comprise

(i) specification of the electric potential at the gate contact:
$$\psi = V_{gs} - V_{fb} \text{ at } x_1 = -t, \tag{7}$$
where V_{fb} is the 'flat-band voltage', which is a voltage that results from terminal contacts with the substrate [2].

(ii) continuity of electric potential and electric displacement at the oxide-substrate interface:

$$\psi^- = \psi^+ \quad \text{and} \quad \epsilon_i \frac{\partial \psi^-}{\partial x_1} = \epsilon_s \frac{\partial \psi^+}{\partial x_1} \text{ at } x_1 = 0. \tag{8}$$

(iii) specification of the electric and quasi-Fermi potentials at the source-substrate and drain-substrate boundaries. These are given in [4], and will not be written out here. They are required for the specification of ψ, φ_n at these boundaries, and they will be introduced when needed subsequently.

(iv) current flow occurs only across the source-substrate and drain-substrate boundaries. A consequence of this is that that the total current flowing across a plane $x_2 = \text{const}$ does not vary with x_2 for $0 \le x_2 \le L$.

The independent and dependent variables are scaled, see Appendix B. With this scaling, the governing equations, (2–4), become

$$\left.\begin{aligned} &\tilde{\nabla}^2 w = \frac{1}{\lambda}\left[\exp((w-\varphi)\log\lambda) - \exp(-w\log\lambda)\right] + d(x) \\ &\tilde{\nabla}^2\varphi + \tilde{\nabla}\varphi \cdot \left(\frac{1}{\mu}\tilde{\nabla}\mu + \log\lambda\,\tilde{\nabla}(w-\varphi)\right) = 0 \\ &\text{where } \tilde{\nabla} \equiv \left(\frac{\partial}{\partial x}, \epsilon\frac{\partial}{\partial y}\right) \end{aligned}\right\}. \tag{9}$$

The differential scaling of the independent variables introduces the parameter ϵ, Equation (1), into the field equations, (2) and (4). The quasi-one-dimensional approximation is obtained for the solution in the mid-channel region (away from the source and drain corners) by the asymptotic expansion for the scaled electric and quasi-Fermi potentials

$$w(x, y) = w^0(x, y) + \epsilon^2 w^1(x, y) + \cdots, \tag{10}$$

$$\varphi(x, y) = \varphi^0(x, y) + \epsilon^2 \varphi^1(x, y) + \cdots. \tag{11}$$

The electron mobility in (3) is not necessarily constant: it may vary spatially and with field strength. The Ward assumption is

$$\mu_n = \mu_n(x, \frac{\partial \varphi^0}{\partial y}) > 0. \tag{12}$$

To leading order

$$\frac{\partial^2 w^0}{\partial x^2} = \frac{1}{\lambda}(\exp((w^0 - \varphi^0)\log(\lambda)) - \exp(-w^0\log(\lambda)) + d(x), \tag{13}$$

$$\frac{\partial^2 \varphi^0}{\partial x^2} = -\left(\frac{1}{\mu_n}\frac{\partial \mu_n}{\partial x} + \log(\lambda)\left(\frac{\partial w^0}{\partial x} - \frac{\partial \varphi^0}{\partial x}\right)\right)\frac{\partial \varphi^0}{\partial x}. \tag{14}$$

The equation for φ^0 can be integrated, and with the no-flux boundary condition it follows that

$$\frac{\partial \varphi^0}{\partial x} = 0 \quad \text{and} \quad \varphi^0 = \varphi(y), \tag{15}$$

where we have dropped the zero superscript for convenience.

The order ϵ^2 terms give for φ^1

$$\frac{\partial^2\varphi^1}{\partial x^2}+\left(\frac{1}{\mu_n}\frac{\partial\mu_n}{\partial x}+\log(\lambda)\frac{\partial w^0}{\partial x}\right)\frac{\partial\varphi^1}{\partial x}=-\left(\varphi''+\left(\frac{1}{\mu_n}\frac{\partial\mu_n}{\partial y}+\log(\lambda)\left(\frac{\partial w^0}{\partial y}-\varphi'\right)\right)\varphi'\right), \tag{16}$$

where primes represent derivatives with respect to y. By means of an integrating factor

$$\begin{aligned}&\frac{\partial}{\partial x}\left(\mu_n\exp(\log(\lambda)w^0)\frac{\partial\varphi^1}{\partial x}\right)=\\&\quad=-\mu_n\exp(\log(\lambda)w^0)\left(\varphi''+\left(\frac{1}{\mu_n}\frac{\partial\mu_n}{\partial y}+\log(\lambda)\left(\frac{\partial w^0}{\partial y}-\varphi'\right)\right)\varphi'\right).\end{aligned} \tag{17}$$

If we integrate each side of (17) from $x = x^*$ (x^* is a point in the substrate where there is no current flux across $x = x^*$) we obtain for the left-hand side

$$\left[\left(\mu_n\exp(\log(\lambda)w^0)\frac{\partial\varphi^1}{\partial x}\right)\right]_0^{x^*}=0, \tag{18}$$

as $\partial\varphi^1/\partial x = 0$ when $x = 0$ and $x = x^*$. It follows that we must have

$$\varphi''+\frac{\partial}{\partial y}\log\left(\int_0^{x^*}\mu_n\exp(\log(\lambda)(w^0-\varphi))\,\mathrm{d}x\right)\varphi'=0. \tag{19}$$

The notation

$$\sigma_m=\int_0^{x^*}\mu_n\exp(\log(\lambda)(w^0-\varphi))\,\mathrm{d}x \tag{20}$$

allows the equation determining the y dependence of φ to be integrated once to give

$$\varphi'\sigma_m\log(\lambda)=C. \tag{21}$$

3. Ward's $\lambda \gg 1$ asymptotic expansion

We copy the 1-D scaled charge conservation equation, (13), written in the form

$$\begin{aligned}w_{xx}=\ &\exp((w-\varphi-1)\log\lambda)\ -\exp(-(w+1)\log\lambda)\ +1\quad\text{for } x>0.\\&(i)\qquad\qquad(ii)\qquad\qquad\quad(iii)\qquad\quad(iv)\end{aligned} \tag{22}$$

The second line provides notation for the identification of terms: terms (i–iv) on the RHS represent charge densities due to electrons, holes and the static impurity doping, respectively. The impurity doping is taken to be constant: for an n-channel device and with the scaling adopted in Appendix B, it has the value unity. The electric potential, w, asymptotes to the value $w = -1$ in the substrate (terms (iii) and (iv) balance) and this provides the boundary condition at large x. There are no charges in the oxide layer, $-t < x_1 < 0$, giving a potential linear in x. This together with the boundary condition that the potential is $V_{gs}-V_{fb}$ at $x_1 = -t$ and the continuity of electric displacement at $x = 0$ means that the latter can be written

$$\left.\frac{\partial w}{\partial x}\right|_s=c_{ox}\sqrt{\frac{\log\lambda}{\lambda}}(w_s-V_{gs}^*), \tag{23}$$

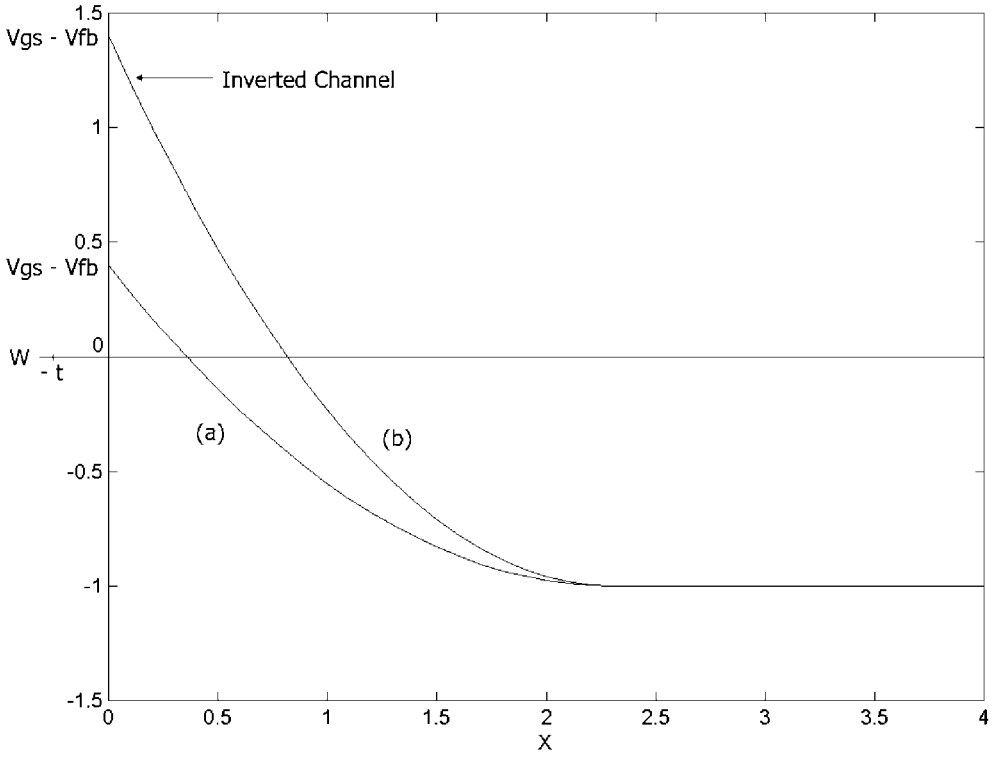

Figure 2. The function $w(x)$ in (a) depletion and (b) inversion.

where s refers to values taken at $x = 0^+$. Figure 2 indicates $w(x)$. (See also Figure 2 in [4].)

In Equation (22) φ is a function only of y which is determined subsequently. Equation (22) allows one integration which together with the boundary condition in the substrate yields

$$\tfrac{1}{2}w_x^2 = \left\{\exp\left[w - \varphi - 1)\log\lambda\right] + \exp\left[-(w+1)\log\lambda\right]\right\} / \log\lambda + w + 1 + 0(\lambda^{-2}). \quad (24)$$

Evaluating this at $x = 0^+$ relates w_s, w_{xs} and φ while (23) relates w_s, w_{xs} and V_{gs}^*. Elimination of w_{xs} yields a relation between w_s, φ and V_{gs}^*. The formula for the current requires $w_s(\varphi)$ in an integration. Hence this may be accomplished numerically.

An alternative to the procedure just outlined is to solve (22) by the method of matched asymptotic expansions. In this, the spatial domain is separated into λ-dependent regions in which various terms in (22) may be neglected. More amenable solutions are achieved, then suitably 'matched'. There are three regimes of operation depending on whether term (ii) is totally absent, present, or present only over part of the y domains. Since $\varphi(0) = 0, \varphi(1) = V_{ds}/V_{th}\log\lambda$, and $\varphi(y)$ is monotonic, the first two regimes categorize easily:

3.1. WEAK INVERSION – DEPLETION:

$$-1 < w_s < 1 + \frac{V_{ds}}{V_{th}\log\lambda}, \quad \text{for all} \quad y, \quad (25)$$

3.2. STRONG INVERSION:

$$w_s > 1 + \frac{V_{ds}}{V_{th}\log\lambda}, \quad \text{for all} \quad y. \quad (26)$$

The last regime has part of the device (adjacent to the source) in strong inversion and part (adjacent to the drain) in weak inversion-depletion and the change-over depends on $\varphi(y)$. This is called pinch-off. When the pinch-off location is designated by the subscript, po, the third regime is:

3.3. PINCH OFF: WEAK INVERSION – DEPLETION

$$-1 < w_s < 1 + \varphi_{po}, \quad \text{for} \quad y_{po} < y < 1. \tag{27}$$

In the weak inversion-depletion regime there is an x-domain adjacent to $x = 0$ in which the dominant terms in (22) are (i) and (iv). This solution must be matched to the solution in the substrate via a transition layer (in which (i) = (iii) + (iv)). Note that φ plays no role in this solution. In the strong inversion regime there is an x-domain adjacent to $x = 0$ in which the dominant terms in (22) are (i) and (ii). (The latter term represents proliferation of electrons in a narrow layer near $x = 0$ – the channel – and it is flow of these electrons along the channel that gives strong current flow). This inverted region must be matched to a depletion solution and at larger x to the substrate solution. All these solutions and matchings are obtained in Ward; only the results will be quoted here.

3.4. STRONG INVERSION REGIME: $w_s > 1 + \varphi$

From the solution given in [4], Equation (6.1),

$$\frac{\partial w}{\partial x}|_s = -\sqrt{2}\alpha_0 \coth\gamma, \tag{28}$$

where

$$\alpha = \sinh\gamma, \;\; \alpha = \alpha_0(\log\lambda)^{1/2}\lambda^{(1-w_s+\varphi)/2}, \tag{29}$$

$$\alpha_0^2 = 2 + \varphi + K - 1/\log\lambda, \tag{30}$$

$$K = \frac{\log(\log\lambda)}{\log\lambda} + \frac{2}{\log\lambda}\left[\log(2\alpha_0) - \gamma\right]. \tag{31}$$

3.5. PINCH-OFF: ASYMPTOTIC SOLUTION

In the pinch-off regime a portion of the device is in weak inversion-depletion. The asymptotic solution ([4, Section 4.1]) is substituted in the boundary condition (23) giving

$$(w_s)_{po} = V_{gs}^* + \frac{1}{c^2\log\lambda} - \frac{1}{c^2\log\lambda}\left\{2c^2\log\lambda\left(V_{gs}^* + 1 - \frac{1}{\log\lambda}\right) + 1\right\}^{1/2}. \tag{32}$$

Since the device becomes inverted for $w_s > 1 + \varphi$ (term (ii) on the right-hand side of (22) becomes dominant) the pinch-off boundary is at φ_{po} where

$$\varphi_{po} = (w_s)_{po} - 1. \tag{33}$$

The asymptotic solution (28) is a replacement for the exact relations between w_s,w_{xs} and φ obtained from (24). The elimination of w_{xs} from (23) and (28) to generate $w_s(\varphi)$ remains a numerical task; Sarvas and Spanier, [12], obtained results by Newton iteration. In the following section we take the asymptotics a little further so that $w_s(\varphi)$ is obtained in analytic form.

4. Further asymptotics

If we combine the expressions for α_0 and K in (29–31) we obtain

$$\alpha_0^2 = 2 + \varphi + \frac{\log(\log\lambda)}{\log(\lambda)} + 2\frac{\log(2\alpha_0) - \gamma - \frac{1}{2}}{\log(\lambda)}. \tag{34}$$

Using the definition of γ, we can write this as

$$\alpha_0^2 = 2 + \varphi + \frac{\log(\log\lambda)}{\log(\lambda)} + \frac{2}{\log(\lambda)}\log\left(2\frac{z\sqrt{\log(\lambda)}}{1+\sqrt{\frac{z^2}{\alpha_0^2}\log(\lambda)+1}}\right) - \frac{1}{\log(\lambda)}, \tag{35}$$

where

$$z = \alpha_0/\alpha\sqrt{\log\lambda}. \tag{36}$$

Also we write

$$c_{ox} = c\sqrt{\lambda}. \tag{37}$$

In Ward $c_{ox} = 450$, and in the data supplied by ISI $c_{ox} = 1244$; for $\lambda \backsim 10^6$ this gives c to be an $O(1)$ quantity.

Elimination of w_{xs} between (23) and (28), and use of (37) yields

$$\left\{2\left(1 + \alpha_0^2\log\lambda\ \ \lambda^{1-w_s+\varphi}\right)\right\}^{1/2}\lambda^{(w_s-1-\varphi)/2} = c\log\lambda(V_{gs}^* - w_s). \tag{38}$$

This complicated relationship between w_s and φ can be solved by iteration. It is convenient to introduce the notation:

$$r = w_s - 1 - \varphi,\ s = V_{gs}^* - 1 - \varphi,\ z = \lambda^{r/2}/\log\lambda. \tag{39}$$

We have noted above that $z = \alpha_0/\alpha\sqrt{\log\lambda}$, but it helps to keep the notation just introduced.

With the substitutions (39), Equation (38) reads

$$\sqrt{2(z^2 + \alpha_0^2/\log\lambda)} = c\left(s - 2\frac{\log\log\lambda}{\log\lambda} - \frac{2\log z}{\log\lambda}\right). \tag{40}$$

Since $\log\lambda \gg 1$, an iterative solution to (35) and (40) can be constructed in the following way. Define the sequences $\{\beta_j\}_{j=0}^{\infty}$ and $\{z_j\}_{j=0}^{\infty}$ by the recurrence formulae

$$\beta_{j+1}^2 = 2 + \varphi + \frac{\log(\log\lambda)}{\log(\lambda)} + \frac{2}{\log(\lambda)}\log\left(2\frac{z_j\sqrt{\log(\lambda)}}{1+\sqrt{\frac{z_j^2}{\beta_j^2}\log(\lambda)+1}}\right) - \frac{1}{\log(\lambda)}, \tag{41}$$

$$z_{j+1} = \frac{c}{\sqrt{2}}\left(s - 2\frac{\log(\log\lambda)}{\log(\lambda)} - 2\frac{\log(z_j)}{\log(\lambda)}\right)\left(1 + \frac{\beta_j^2}{z_j^2\log(\lambda)}\right)^{-\frac{1}{2}} \tag{42}$$

for $j \geq 0$, and start the sequences with the values

$$\beta_0^2 = 2 + \varphi + \frac{\log(\log\lambda)}{\log(\lambda)}, \tag{43}$$

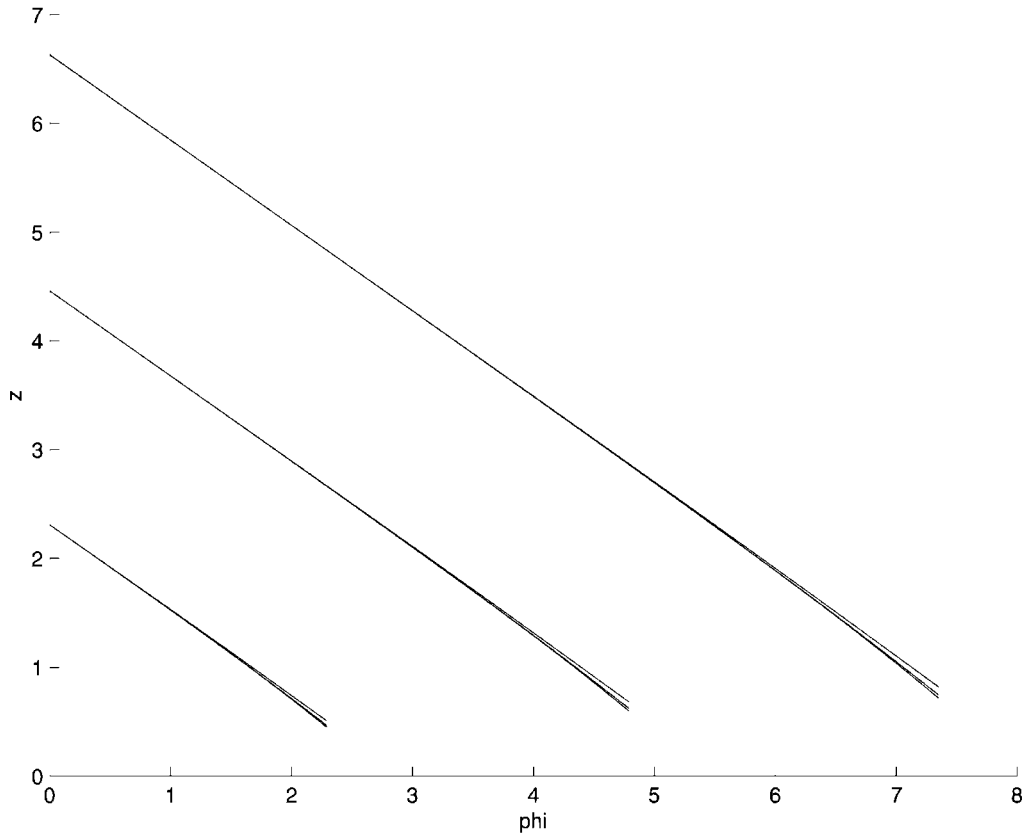

Figure 3. The first three iterations for (left to right) $V_{gs} = 1, 2, 3$ V.

$$z_0 = \frac{c}{\sqrt{2}}(s - 2\frac{\log(\log\lambda)}{\log(\lambda)}). \tag{44}$$

Provided these sequences are convergent we have

$$z_j \to z \text{ and } \beta_j \to \alpha_0 \text{ as } j \to \infty. \tag{45}$$

These values of z give r and hence w_s, in terms of s, and hence φ, with V_{gs}^* as a parameter.

Figure 3 shows the first three iterations (z_1 to z_3) given by the iterative scheme for (41 –42), and shows excellent convergence to the exact solution. The latter (not shown) was obtained from Sarvas and Spanier, [12], who solved (23), (24) numerically (and provided us with the MATLAB programs to reproduce their results). The scheme has effectively converged at z_3. These calculations relate only to the inverted region: that is, Figure 3 shows calculations terminated at φ_{po} given by (33).

The fast iteration shown in Figure 3 enables us to generate explicit formulae for the solution. For instance, the first iterate, z_1, is a reasonable approximation to the exact solution, and it can be written in a formula taking up only a couple of lines.

Using the iterative solution for z the relation $w_s(\varphi)$ may be obtained from the relations (39) in the inverted region, and $(w_s)_{po}$ from (32) extends it for $\varphi > \varphi_{po}$. These results are shown in Figure 4 for $\overline{V}_{gs} = 70, 80, 90,$ respectively.

The approximations pre-and post-pinch-off have been blended by use of the blending Y, see Appendix D. Also shown (circles) are the exact results obtained in [12], which indicate

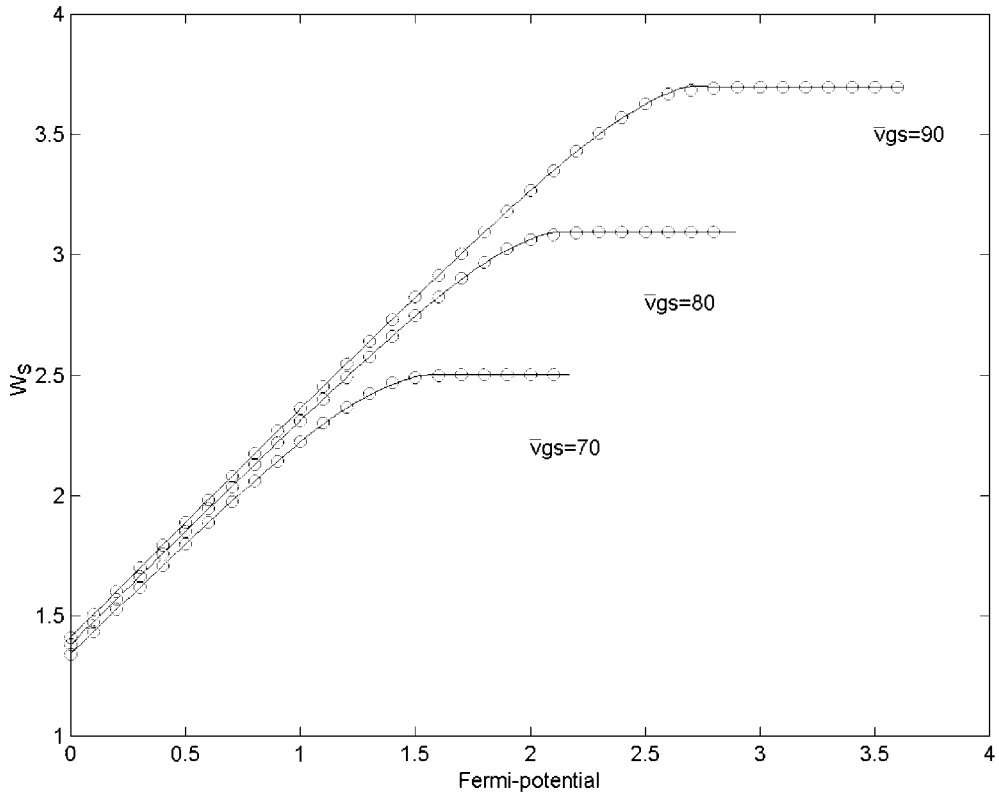

Figure 4. $w_s(\varphi)$ for $\overline{V}_{gs} = 70, 80, 90$.

that a very high level agreement between the asymptotic and exact numerical approaches has been achieved.

5. Current

The definition of the quasi-Fermi potential φ_n, (6), allows the current flux $\mathbf{J}_n$, (3), to be expressed as

$$\mathbf{J}_n = q\mu_n \frac{kT}{q} n \nabla \varphi_n. \tag{46}$$

The current flowing from source to drain, I_{ds}, is obtained:

(a) by first integrating the x_2 - component of $\mathbf{J}_n$ in the x_1-direction to obtain the current flowing across a plane x_2 = a constant. We may evaluate this integral, using the asymptotic representation of the solution, [4].

(b) by performing a second integration in the x_2-direction from source to drain.

Since, as has been noted already, the current across a plane x_2 = constant does not vary with x_2, this integration of I_{ds} yields on the left-hand side LI_{ds}, whilst on the right-hand side the conjunction $\frac{\mathrm{d}\varphi_n}{\mathrm{d}x_2} dx_2 = \mathrm{d}\varphi_n$ yields an integration with respect to φ_n. Since the solution is known in terms of φ_n, this artifice avoids determining φ_n as a function of x_2.

We obtain expressions for I_{ds} in the regimes when the whole device is inverted, and when it is in pinch-off (partially inverted, partially depleted).

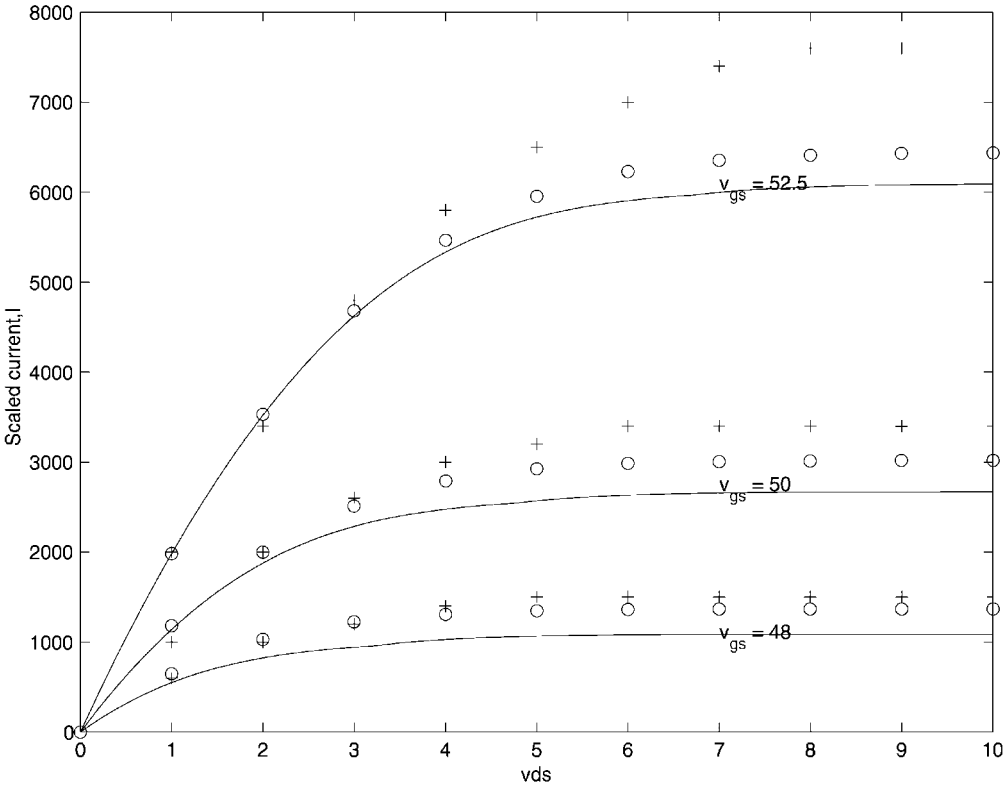

Figure 5. The scaled current for $\overline{V}_{gs} = 48, 50, 52{\cdot}5$ (For $\lambda = 10^6$).

5.1. LINEAR REGIME

When the whole device is inverted the current rises approximately linearly with V_{ds} : hence the title. For constant mobility the current is found from [4, Equations (3.6,7), (6.5,6)] as

$$\frac{I_{ds}}{\mu I_c} = \sqrt{2}\log\lambda \int_0^{\overline{V}_{ds}/\log\lambda} \exp\left[\frac{1}{2}(w_s - \varphi)\log\lambda - \gamma\right] \mathrm{d}\varphi. \tag{47}$$

The substitutions (39) allow us write the current integral in the form

$$\frac{I}{\mu I_c} = \sqrt{2\lambda}(\log(\lambda))^2 \int_{z_d}^{z_s} H(z, \alpha_0^2(z))\mathrm{d}z, \tag{48}$$

where

$$H(z, \alpha_0^2(z)) = z\frac{\mathrm{d}s}{\mathrm{d}z}\mathrm{e}^{-\gamma}. \tag{49}$$

Equation (40) yields

$$\frac{\mathrm{d}s}{\mathrm{d}z} = \left\{\frac{\sqrt{2}}{c}\frac{z}{\sqrt{z^2 + \alpha_0^2/\log\lambda}} + \frac{2}{z\log\lambda}\right\}\left\{1 + \frac{1}{c\log\lambda(2z^2 + 2\alpha_0^2/\log\lambda)^{1/2}}\right\}^{-1}. \tag{50}$$

Using the relations (28−31) we can express

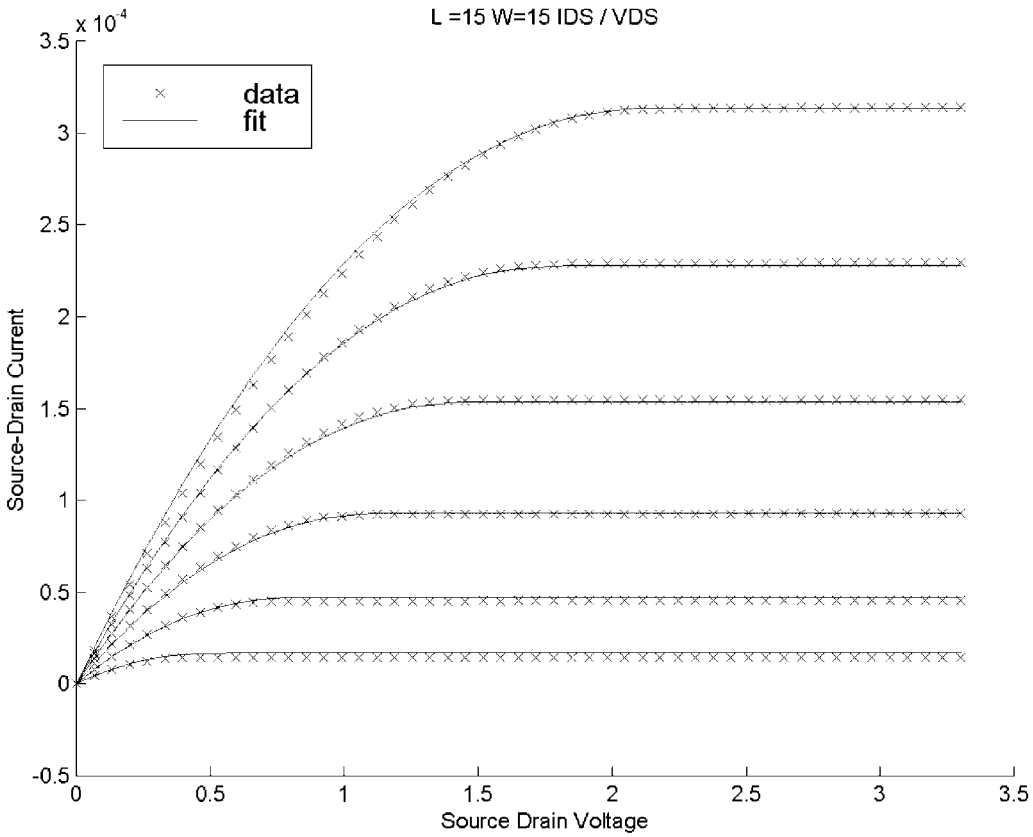

Figure 6. A long $L = 15$ and width $W = 15$ device ($\lambda = 10^7$).

$$e^{-\gamma} = (1 + \alpha_0^2/z^2 \log \lambda)^{1/2} - \alpha_0/z\sqrt{\log \lambda}. \tag{51}$$

The functions ds/dz and $e^{-\gamma}$ can be seen to be decreasing functions of α_0^2 for fixed z by direct observation of their functional forms in (50) and (51). Consequently, the current integrand $H(z, \alpha_0^2(z))$ is monotonically decreasing as a function of α_0^2 for fixed z. The function $\alpha_0^2(z)$ is similarly monotonically decreasing and bounded on $[z_d, z_s]$

$$m \leq \alpha_0^2(z) \leq M \quad \text{for} \quad z \in [z_d, z_s]. \tag{52}$$

Define the function

$$W(t) = \int_{z_d}^{z_s} H(z, t)dz \quad \text{for} \quad t \in [m, M]. \tag{53}$$

This is monotonic in t and lies in the interval $[W(M), W(m)]$. As $H(z, \alpha_0^2(z))$ is monotonically decreasing as a function of α_0^2 for fixed z we can write

$$W(M) \leq \int_{z_d}^{z_s} H(z, \alpha_0^2(z))dz \leq W(m). \tag{54}$$

By the intermediate-value theorem there is a value of t for which $W(t)$ takes any value in $[W(M), W(m)]$. In particular there is a value $t = t^* \in [m, M]$ for which

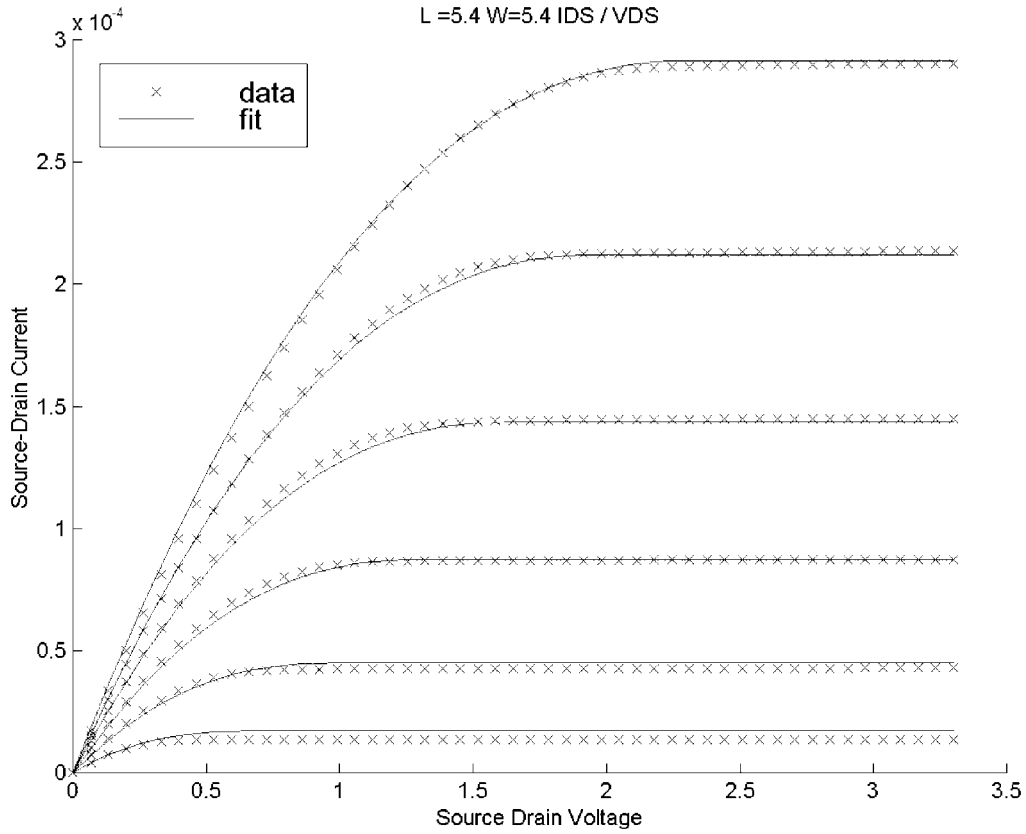

Figure 7. A $L = 5{\cdot}4$ and width $W = 5{\cdot}4$ device ($\lambda = 10^7$).

$$\int_{z_d}^{z_s} H(z, \alpha_0^2(z))\,\mathrm{d}z = \int_{z_d}^{z_s} H(z, t^*)\,\mathrm{d}z. \tag{55}$$

As $\alpha_0^2(z)$ is monotonic decreasing on $[z_d, z_s]$ there exists a $z^* \in [z_d, z_s]$ for which

$$\alpha_0^2(z^*) = t^* = \overline{\alpha}_0^2 \tag{56}$$

From (35) the equation for $\overline{\alpha}_0^2$ is

$$\begin{aligned}\overline{\alpha}_0^2 = {} & 1 + V_{gs}^* - \frac{\sqrt{2}}{c}\sqrt{(z^*)^2 + \frac{\overline{\alpha}_0^2}{\log(\lambda)}} - \frac{\log(\log\lambda)}{\log(\lambda)} + \\ & + \frac{2}{\log(\lambda)}\log\left(\frac{2}{\sqrt{e}}\frac{\sqrt{\log(\lambda)}}{1 + \sqrt{\dfrac{(z^*)^2}{\overline{\alpha}_0^2}\log(\lambda) + 1}}\right)\end{aligned} \tag{57}$$

which can be written in the form

$$\overline{\alpha}_0^2 = P - \frac{\sqrt{2}}{c}\sqrt{(z^*)^2 + \frac{\overline{\alpha}_0^2}{\log(\lambda)}}, \tag{58}$$

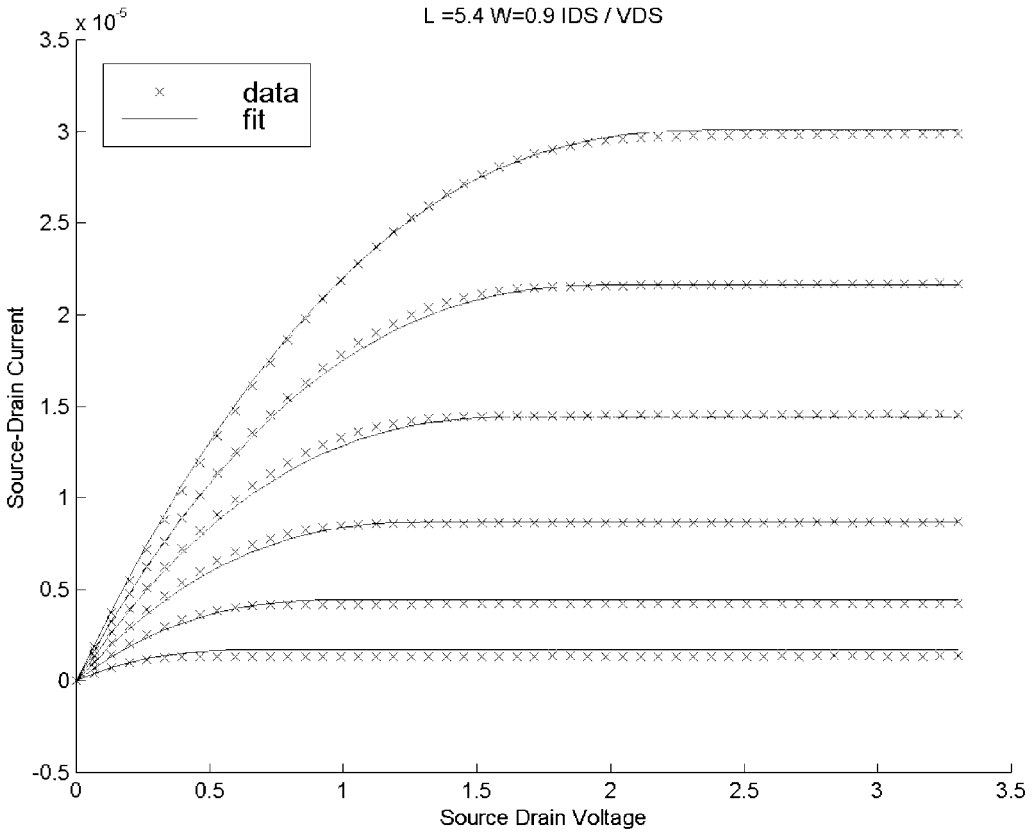

Figure 8. A $L = 5{\cdot}4$ and width $W = 0{\cdot}9$ device ($\lambda = 10^7$).

involving

$$P = 1 + V_{gs}^* - \frac{\log(\log\lambda)}{\log(\lambda)} + \frac{\kappa}{\log(\lambda)} \tag{59}$$

and

$$\kappa = 2\log\left(\frac{2}{\sqrt{e}}\frac{\sqrt{\log(\lambda)}}{1+\sqrt{\frac{(z^*)^2}{\overline{\alpha}_0^2}\log(\lambda)+1}}\right). \tag{60}$$

Assuming that z^* is small, we can write the solution for $\overline{\alpha}_0$ in the form

$$\overline{\alpha}_0^2 \backsim P - \frac{\sqrt{2}}{c}\sqrt{\frac{P}{\log(\lambda)}} \tag{61}$$

with P given by (59). The unknown value z^* has a dependence upon V_{gs}^* but this is expected to be weak. In the fitting process (see Section 6) κ is treated as a free parameter and determined by the least-squares optimization process. As α_0 can be treated as a constant $\overline{\alpha_0}$ in (48) the integral can be evaluated explicitly. Having done this, we obtain the final result for the current in the linear regime, which is

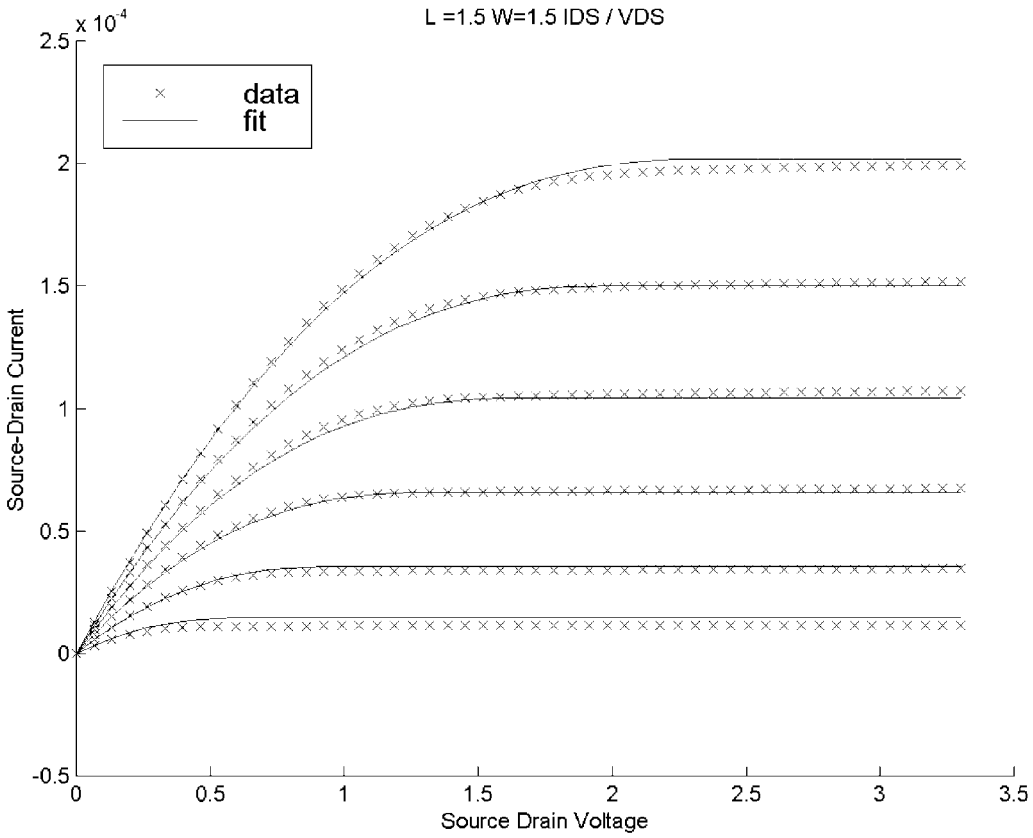

Figure 9. A $L = 1{\cdot}5$ and width $W = 1{\cdot}5$ device ($\lambda = 10^7$).

$$\frac{I_{ds}}{\mu I_c} = \left\{2\lambda(\log\lambda)^3\right\}^{1/2}\overline{\alpha_0}\left\{I\left(\frac{z_s\sqrt{\log\lambda}}{\overline{\alpha_0}}\right) - I\left(\frac{z_d\sqrt{\log\lambda}}{\overline{\alpha_0}}\right)\right\}, \tag{62}$$

where $I(x)$ is defined by

$$\begin{aligned} I(x) \;=\; & \frac{\overline{\alpha_0}}{c}\sqrt{\frac{2}{\log\lambda}}\left(\frac{1}{2}y^2 - \beta^2 y + \beta^4\log(y+\beta^2)\right) + \\ & + \frac{2}{\log\lambda}\left(y + \frac{\log(y-1)}{2(1+\beta^2)} - \frac{\log(y+1)}{2(1-\beta^2)} + \frac{\beta^6}{1-\beta^4}\log(y+\beta^2)\right) - \\ & - \frac{\overline{\alpha_0}}{c}\sqrt{\frac{2}{\log\lambda}}\left(y - \beta^2\log(y+\beta^2)\right) - \\ & - \frac{2}{\log\lambda}\left(\frac{\log(y-1)}{2(1+\beta^2)} + \frac{\log(y+1)}{2(1-\beta^2} + \frac{\beta^4}{\beta^4-1}\log(y+\beta^2)\right) \end{aligned} \tag{63}$$

where $y = \sqrt{1+x^2}$ and $\beta^2 = 1/c\overline{\alpha_0}\sqrt{2\log\lambda}$.

5.2. SATURATED REGIME

When V_{ds} is large enough a region near the drain changes from inverted to depleted. In this region the elevated values of φ eliminate from importance term (ii) in Equation (22) and the results used for inverted $w_s(\varphi)$ are no longer valid. The integral for current is separated into two parts: (1) that valid in the inverted region and available from the results of the previous section, merely substituting z_{po} for z_d in the upper limit in (48), and (2) that valid in the depleted region for which we can use [4, Equations (4.6), (4.7)]. This gives for the current in the saturated regime the formula

$$\begin{aligned}\frac{I_{ds}}{\mu I_c} &= \left\{2\lambda(\log\lambda)^3\right\}^{1/2}\overline{\alpha}_0\left\{I\left(\frac{z_s\sqrt{\log\lambda}}{\overline{\alpha}_0}\right) - I\left(\frac{z_{po}\sqrt{\log\lambda}}{\overline{\alpha}_0}\right)\right\} + \\ &\quad Q_c\left(\exp\left(-\overline{V}_{ds}\right) - \exp\left(-\varphi_{po}\log\lambda\right)\right),\end{aligned} \tag{64}$$

where $I(x)$ is given by (63), and φ_{po} is given by (33), and Q_c is given by (see [4, Equation (4.7)]:

$$Q_c = -\mathrm{e}^{w_s\log\lambda}(2\lambda\log\lambda)^{-\frac{1}{2}}(w_s + 1 - 1/\log\lambda)^{-\frac{1}{2}}\left(1 + \frac{1}{2(w_s + 1 - 1/\log\lambda)\log\lambda}\right) \tag{65}$$

with w_s taking the value w_{spo}.

Figure 5 shows the scaled drain current I_{ds} as a function of $\overline{V}_{ds}$ for values of $\overline{V}_{gs} = 48$, 50, 52·5. The + are Ward results, 0 are Spanier and Sarvas numerical results [12], and − are the results of the calculations reported on here.These curves were obtained by blending the current in the linear region, (62), with that in the saturated region (65). The three approaches have the same shape as experimental data, but provide slightly different amplitudes. This is attributed to the following:

Comment 1: Since the agreement between our results and Sarvas and Spanier has been excellent so far, the difference in the results for current is attributed to the approximations made in generating the explicit formula (62) from the integral (47).

Comment 2: Divergence between the Sarvas and Spanier and Ward current results was also shown in [12]. The results generated in this paper show the possible source of the differences. Ward states 'γ is transcendentally small' and 'α is transcendentally small in $\log\lambda$' in the linear regime, and bases some approximations on these assertions. However the $w_s(\varphi)$ relation (see Figures 4 and 5) give $w_s - 1 - \varphi \cong 0{\cdot}4$ and this gives

$$\alpha = \alpha_0\sqrt{\log\lambda}\ \ \lambda^{-0{\cdot}2}. \tag{66}$$

There is a negative power of λ in α, but it is small. Since $\alpha = \alpha_0/z\sqrt{\log\lambda}$ and z is 0(1) over a substantial portion of the linear regime (see Figure 3), $\alpha = 0(1/\sqrt{\log\lambda})$ there, and may not be neglected without some penalty.

6. Optimized fitting

A number of assumptions have been made in constructing the model of the MOSFET that has been used. It has been supposed that the mobility μ is a constant in the sense that it is independent of z. It does, however, have a dependence upon V_{gs}^* that must be taken into account if we are to compare our formulae to real data. A common form used in SPICE is given by

$$\mu = \frac{1}{1 + \theta(V_{gs} - V_T)} \tag{67}$$

and we adopt this also. The mobility scaling factor μ_0 is also a parameter that has to be provided in SPICE and our model. These parameters can be extracted from experimental data but it is best to regard such extracted values as estimates. We shall take both these physical parameters, θ and μ_0, as fitting parameters to be determined by the optimization process. In Section 5 we were able to make a partial evaluation of the integrals by invoking the intermediate value theorem. This required the introduction of an additional non-physical parameter z^*. Although this cannot be extracted from the data we do have a sense of its value as it must lie in $[z_d, z_s]$ which we can estimate. Thus we have three variables and approximate values from which to start an optimization process to obtain the best fit to the data. The method of least squares implemented in the form of the Marquardt algorithm, [13], is used to determine the values of these three parameters. We should remark that a similar parameter optimization technique is used in SPICE. None of the physical parameters is known well enough for typical fabricated devices to warrant any alternative approach.

Using 0·35 micron technology data provided by ISI we have applied our method to a number of devices of different channel length and width. Each device was separately fitted. We present the results as a series of plots. Figure 6 is a long and wide device for which we would expect the best agreement.

The fit is excellent. This continues to be true as the channel length and width are reduced. Figure 7 shows a 5·4 micron length device with width 5·4 microns.
As figure 8 shows we can even reduce the width to 0·9 microns still retain an acceptable fit. The fits remain good down to about 1·5 microns as shown by Figure 9.
At shorter lengths the experimental I-V curves develop a non-zero asymptotic slope and are outside the range of validity of our assumptions.

7. Concluding remarks

Explicit formulae for the dependence of current flow on applied voltages and device geometry, doping, etc., have been obtained for the standard MOSFET by asymptotic analysis. The analysis is valid for long channel devices (ϵ, the aspect ratio, Equation (1), small), and for large λ, where λ is the ratio of the doping level to its intrinsic level. However, comparison of the results with experimental data shows that accuracy is maintained for a more extended range of values of ϵ.

The results obtained here extend the work of Ward [4] and generate *explicit* formulae for the current. These formulae are derived directly from the physics of the drift-diffusion model. Ad-hoc assumptions are at a minimum. (Only the mobility has an empirically based dependence). However, some (three) parameters are given values determined by optimally fitting the derived formule with the data; this, though, is standard in the industry. The formulae, though complicated, provide a much simpler model than the ones currently used in industry which require up to 200 fitting parameters.

The semiconductor industry continues to minaturise the device–channel lengths of $0{\cdot}18\mu$ are being fabricated commercially. At this value the aspect ratio is $\epsilon = 2/3$. Hence a two-dimensional theory would be valuable. An asymptotic 2-D scheme along the lines suggested by Ward [5] and realised only in the zero-current case, seems to be the only choice if explicit results are required. This, in the case of non-zero current flow, is a challenging problem.

Acknowledgements

We wish to acknowledge Cesar Piña and Vance Tyree of the University of Southern California Information Sciences Institute for technical discussions and for provision of the MOSFET data that was used in this study.

Appendix

A. Primary Notation and Symbols

x_1, x_2	co-ordinates along and perpendicular to channel (See Figure 1)	ρ	is the space charge density
L, W	are channel length and width	n_i	is the intrinsic carrier concentration
t	is oxide thickness	q	is the charge of a proton
n, p	are the electron and hole concentrations	k	is the Boltzmann's constant
N	is the concentration of selected impurities or dopants	T	is the lattice temperature (assumed constant)
$\mathbf{J}_n$	is the electron current density	$V_{th} = kT/q$	is called the thermal voltage
$\mathbf{E}$, ψ	are the electric field and electrostatic potential	V_T	is the threshold voltage, a measurable characteristic of the device
ϕ_n	is the quasi-Fermi potential for electrons	$L_D = \left(\frac{kT\varepsilon_s}{n_i q^2}\right)^{\frac{1}{2}}$	is called the Debye length
μ_n, μ_0	are the electron mobility, typical mobility magnitude	V_{ds}	is drain-to-source voltage
ε_s	is the dielectric constant of the semiconducting material	V_{gs}	is gate-to-source voltage
ε_i	is the dielectric constant of the oxide insulator	V_{fb}	is flat-band voltage
I_{ds}	is the source-to-drain current		

B. Scaled Variables

$$\lambda = \max|N(x_1)/n_i| \qquad c_{ox} = \varepsilon_i L_D/\varepsilon_s t$$
$$x_1 = L_d\left(\frac{\log\lambda}{\lambda}\right)^{1/2} x \qquad x_2 = Ly \qquad c = c_{ox}/\sqrt{\lambda}$$
$$d(x) = N(L_D(\tfrac{\log\lambda}{\lambda})^{1/2}x)/n_i \qquad V_{gs} - V_{fb} = V_{th}(\overline{V}_{gs} - \log\lambda) = V_{th}\log\lambda \;\; V^*_{gs}$$
$$(\psi, \phi_n) = V_{th}\log\lambda \;\; (w, \phi) \qquad V_{ds} = V_{th}\overline{V}_{ds}$$

C. Numerical Values

$L_D = 33$ microns $\quad V_{fb} = -0{\cdot}6$ volt

$V_{th} = 0{\cdot}0259$ volt $\quad \mu_0 = 0{\cdot}0407$ m^2 volt^{-1} s^{-1}

The table below shows the corresponding magnitudes of $\overline{V}_{gs}$ and V_{gs} for $\lambda = 10^6$

$\overline{V}_{gs}$	48	50	52·5	70·0	80·0	90·0
V_{gs} volt	0·2854	0·3372	0·4019	0·8552	1·1142	1·3732

If the value of λ is increased the values of $\overline{V}_{gs}$ are larger. For example if $\lambda = 10^7$ then $\overline{V}_{gs} = 155$ corresponds to $V_{gs} = 2{\cdot}997$ volt.

D. Blending

In the theory of matched asymptotic expansions the construction of two approximate solutions each valid in one of two domains that are contiguous and overlapping is a typical situation. The construction of a composite expansion valid over the union of the domains is then indicated, and there are techniques available prescribing how to accomplish this. The composite expansion (to some order) will be accurate (to that order) uniformly over the whole domain and will have no reduction in smoothness from the component solutions. The desirability of this procedure is evident, and it transcends the domain of asymptotic analysis: one may have separate solutions valid in separate domains that one wishes to join or blend smoothly. These solutions may in some sense be asymptotic – and so complicated that one shrinks at the chore of finding the composite – or not. This section explores some ideas on how to blend such solutions in an empirical, ad-hoc way.

This topic was taken up by Wollkind, [14], and the analysis concerned problems in which (in the language of matched asymptotic expansions) the two component solutions consist of an inner solution valid near a boundary of the domain (a boundary layer) and an outer solution valid elsewhere. We have used the ideas presented by Wollkind to form a blended solution from the asymptotic formulae for separate 'linear' and 'saturated' components.

Let us start the discussion with a simple example. Suppose we have approximations (in $x > 0$)

$$y = \begin{cases} \alpha x & \text{close to } x = 0 \\ 1 & \text{away from } x = 0 \end{cases}. \tag{D1}$$

Following Wollkind, a blended solution is

$$y = (\alpha x - 1)\mathrm{e}^{-x/\epsilon} + 1, \tag{D2}$$

since it has the behavior of (D1), for $x \gg \epsilon$ and for $x \ll \epsilon$. (The Wollkind technique would find ϵ by least squares fitting (D2) to (D1) (αx joined to 1 at $x = 1/\alpha$)). Clearly this procedure gets more accurate the more closely this example resembles a boundary layer problem ($\alpha \gg 1$).

Let us now extend the discussion beyond the boundary layer context. Suppose we have approximations

$$y = L(x),\ R(x) \tag{D3}$$

on the left and right, respectively, of $x = a$. The task is to blend L, R in a smooth formula to provide a blended approximation, $y = Y(x)$.

A first attempt at a blend is given by

$$Y(x) = b_L(x)L(x) + b_R(x)R(x), \tag{D4}$$

$$b_R, b_L = \frac{1}{2}\left\{1 \pm \tanh\frac{x-a}{\epsilon}\right\}.$$

The blending functions b_R, b_L are, for small ϵ, essentially unity in $x \lessgtr a$ and zero in the complement, and use of them assures that Y gives (D3) outside a transition region around $x = a$. Since Y is a convex linear combination of L, R at each x it lies between L and R and provides a blend.

Comments

Choice of ϵ: In problems in which asymptotic series have been developed for $L(x)$, $R(x)$ there will be a small parameter which may be identified with ϵ, in which case L, R have been blended through a suitably chosen transition layer. This is the case in the applications in this paper. In other circumstances, ϵ may have to be determined numerically, say by a least-squares fitting of the blended function to data.

Choice of a: In the theoretical development above, the value of a was determined as the intersection point for L, R. Where L, R do not intersect, or where a may not be found accurately, experimentation or extra numerical procedures may be required in order to determine a in order to arrive at a good blending function.

References

1. A. Massobrio and P. Antognetti, *Semiconductor Device Modeling with SPICE*. New York: McGraw-Hill (1993) 479 pp.
2. S. Sze, *Physics of Semiconductor Devices*. New York: John Wiley (1969) 868 pp.
3. Y. Tsividis, *Operation and Modeling of the MOS Transistor*. New York: McGraw-Hill (1987) 505 pp.
4. M. J. Ward, F. M. Odeh, and D. S. Cohen, Asymptotic methods for metal oxide semiconductor field effect transistor modeling. *SIAM J. Appl. Math* 50 (1990) 1099–1125.
5. M. J. Ward, Singular perturbations and a free boundary problem in the modeling of field-effect transistors. *SIAM J. Appl. Math.* 52 (1992) 112–139.
6. H. Pao and C. Sah, Effects of diffusion current on characteristics of metal-oxide (insulator)-semiconductor transistors. *Solid State Electr.* 10 (1966) 927–937.
7. R. Pierret and J. Shields, Simplified long channel MOSFET theory. *Solid State Electr.* 26 (1983) 143–147.

8. M. Martelli, E. Cumberbatch, A. Klafter, S. Pilorz, R.L. Polosa, G. Ruddock, and A. Smith (for Jet Propulsion Laboratory) Modelling short channel MOSFETS for use in VLSI. Claremont Graduate School Final Clinic Report (May 1986).
9. C. Please, An analysis of semiconductor P-N junctions. *IMA J. Appl. Math.* 28 (1982) 301–318.
10. J. Kevorkian and J. D. Cole, *Multiple Scale and Singular Perturbation Methods*. New York: Springer (1996) 632 pp.
11. P.A. Markowich, C.A. Ringhofer, and C. Schmeiser, *Semiconductor Equations*. Wien, New York: Springer-Verlag (1990) 248 pp.
12. J. Sarvas and J. Spanier, A direct approach to solving the drift-diffusion model equations for use in certain MOSFET devices. *Mathl. Comput. Modelling* 22 (1995) 17–31.
13. D. Marquardt, An algorithm for least-squares estimation of nonlinear parameters. *SIAM J. Appl. Math.* 11 (1963) 431–441.
14. D. J. Wollkind, Singular perturbation techniques: a comparison of the method of matched asymptotic expansions with that of multiple scales. *SIAM Rev.* 19 (1977) 502–516.